Available online at www.sciencedirect.com

ScienceDirect

International Journal of Heat and Mass Transfer 50 (2007) 4967–4974

International Journal of HEAT and MASS TRANSFER

www.elsevier.com/locate/ijhmt

Computation of high Prandtl number turbulent thermal fields by the analytical wall-function

Kazuhiko Suga *

Department of Mechanical Engineering, Osaka Prefecture University, 1-1, Gakuen-cho, Naka-ku, Sakai 599-8531, Japan

Received 9 April 2007; received in revised form 14 September 2007
Available online 7 November 2007

Abstract

The extended version of the analytical wall-function (AWF) for rough wall turbulence by Suga et al. [K. Suga, T.J. Craft, H. Iacovides, An analytical wall-function for turbulent flows and heat transfer over rough walls. Int. J. Heat Fluid Flow 27 (2006) 852–866] is improved for high Prandtl number flows. The original AWF assumes a linear profile of turbulent viscosity near a wall though it is widely recognised that a theoretically correct cubic profile of the turbulent viscosity is essential for heat transfer of high Prandtl number flows. In order to predict thermal boundary layer of high Prandtl number fluid flows, the present approach thus employs a correct limiting profile of the turbulent viscosity in the analytical integration process. The presently proposed version of the AWF proves its good performance for predicting turbulent high Prandtl number thermal flows at $Pr \leqslant 4 \times 10^4$ for smooth wall cases, and at least at $Pr \leqslant 10$ for rough wall cases.

Keywords: Wall-function; Turbulence; High Prandtl number; Heat transfer

1. Introduction

If one considers to predict turbulent wall heat transfer of high Prandtl number (Pr) fluid flows such as cooling oil and IC engine water-jacket flows, it is essential to analyse the thermal boundary-layer which is much thinner than that of the flow boundary-layer. Thus, near-wall modelling which resolves the viscous sub-layer has been thought to be essential for high Pr thermal fields. For example, at the development of a novel turbulent heat flux model applicable to general Pr cases, Rogers et al. [1] supposed correct near-wall stress distribution and Suga and Abe [2] employed a low Reynolds number (LRN) nonlinear $k-\varepsilon$ model. In the context of eddy diffusivity models, Herrero et al. [3] applied an LRN $k-\varepsilon$ model. So and Sommer [4] also applied an LRN $k-\varepsilon$ as well as a near-wall stress transport models for flows at $Pr = 1000$.

However, even with the recent development of LRN heat transfer models, industrial engineers still routinely make use of classical wall-function approaches. (One of the main reasons is a high computational cost of the LRN computation. The difficulty to generate quality near-wall grids for complex three-dimensional flow fields such as IC engine water-jacket flows is another serious problem.) The wall-function strategies most commonly used assume semi-logarithmic variations of the near-wall velocity and temperature (e.g. [5]). It is, however, well known that the reliable performance of those approaches is so limited into relatively simple flows due to those assumptions.

In order to provide a more reliable strategy, the University of Manchester group proposed a new scheme [6] where the near-wall variation of the turbulent viscosity is assumed, from which the mean flow and energy equations are analytically integrated over the near-wall control

* Tel.: +81 72 254 9224; fax: +81 72 254 9904.
E-mail address: suga@me.osakafu-u.ac.jp

0017-9310/$ - see front matter © 2007 Elsevier Ltd. All rights reserved.
doi:10.1016/j.ijheatmasstransfer.2007.09.020

Nomenclature

A_T, A_U, B_T, B_U	integration constants
c_p	specific heat capacity at constant pressure
c_ℓ, c_μ	model constants
C_h	model coefficient
C_T	sum of the convection and the diffusion terms of the energy equation
C_U	sum of the convection and the diffusion terms of the momentum equation
D	channel height
h, h^*	roughness height, equivalent sand grain roughness height, $h\sqrt{k_P}/\nu$
h^+	roughness Reynolds number: hU_τ/ν
k, k_P	turbulence energy, k at node P
P	pressure or cell center of the wall-adjacent cell
Pr	Prandtl number
Pr_t, Pr_t^∞	turbulent Prandtl numbers
q_w	wall heat flux
Re	Reynolds number: U_bD/ν
S_θ	source term of the energy equation
U_b, U_τ, U^+	bulk velocity, friction velocity, U/U_τ
x	wall-parallel coordinate
y	wall normal coordinate or wall normal distance
y_n, y_v, y_b	cell height, viscous sub-layer thicknesses
y^+, y^*	normalised distances: $y\,U_\tau/\nu$, $y\sqrt{k_P}/\nu$
α, α'	$c_\mu c_\ell$, $\alpha(y_b^* - y_v^*)/y_b^{*3}$
α_T, α_θ	$\alpha Pr/Pr_t^\infty$, $\alpha Pr/Pr_t$
Γ_U, Γ_θ	normalised total viscosity and thermal diffusivity
δ_v	origin shift
ε	dissipation rate of k
Θ, Θ^+	mean temperature, $\lvert\Theta - \Theta_w\rvert(\rho c_p U_\tau)/q_w$
Θ_w, Θ_n	wall temperature, temperature at the point n
κ	von Kármán constant: 0.42
μ, μ_t	viscosity, turbulent viscosity
ν, ν_t	kinematic viscosity, kinematic turbulent viscosity
ρ	fluid density

volumes. Since this analytical wall-function (AWF) integrates the transport equations, the effects of the pressure gradient or the heat source term are inherently involved in the function.

Recently, several studies thus have followed this AWF approach [7–9]. The present authors [7] first extended the AWF to include the effects of fine-grain surface roughness for flow and thermal fields. In the validation tests of several rough-wall flows, the AWF showed its performance superior to the standard approach. Its flow and heat transfer results were comparable to those of the LRN solutions by a linear or a nonlinear $k-\varepsilon$ models [10,11].

Although the AWF performs reasonably well at $Pr < 1$ as shown in Fig. 1, its applicability to higher Pr cases was not discussed so far. Therefore, this paper focuses on the improvement of the thermal AWF for high Pr turbulent flows with and without wall roughness.

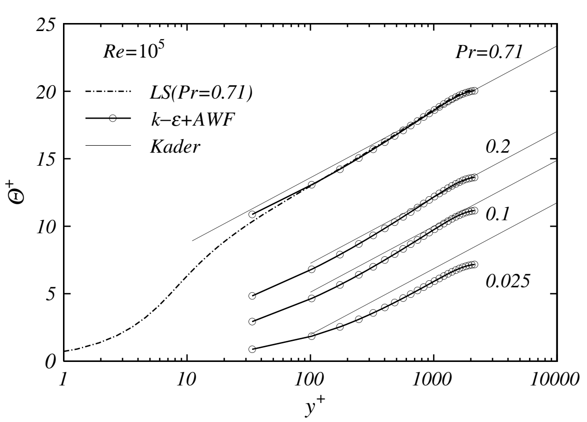

Fig. 1. Mean temperature profiles in turbulent smooth channel flows at $Pr < 1$.

(Note that in the cases shown in Fig. 1, a constant turbulent Prandtl number, $Pr_t = 0.9$, is used for convenience. However, for lower Pr cases, the direct numerical simulation [12] suggested that Pr_t was not constant at all and its level was rather high. There is thus a tendency for the AWF to underpredict the mean temperature profile, particularly, at $Pr = 0.025$. This implies that a functional form for Pr_t is desirable for those cases if one requires better accuracy.)

2. AWF modelling for high Prandtl number flows

2.1. High Pr AWF for smooth wall heat transfer

In the AWF [6], the wall shear stress and heat flux are obtained through the analytical solution of simplified near-wall versions of the transport equations for the wall-parallel momentum and temperature. Using an eddy viscosity concept, those equations can be written as

$$\frac{\partial}{\partial y^*}\left(\mu\Gamma_U\frac{\partial U}{\partial y^*}\right) = \underbrace{\frac{\nu^2}{k_P}\left[\frac{\partial}{\partial x}(\rho UU) + \frac{\partial P}{\partial x}\right]}_{C_U}, \tag{1}$$

$$\frac{\partial}{\partial y^*}\left(\frac{\mu}{Pr}\Gamma_\theta\frac{\partial \Theta}{\partial y^*}\right) = \underbrace{\frac{\nu^2}{k_P}\left[\frac{\partial}{\partial x}(\rho U\Theta) - S_\theta\right]}_{C_T}, \tag{2}$$

where $y^* \equiv yk_P^{1/2}/\nu$, and k_P, y, ν, ρ, P, U, Θ, S_θ, $\mu\Gamma_U$, $\mu\Gamma_\theta/Pr$ are respectively the turbulence energy at the node P, the wall normal direction, the kinematic viscosity, the fluid density, the pressure, the mean wall-parallel velocity component, the mean temperature, a heat source, the total viscosity, the total thermal diffusivity. The main assumption required for the analytical integration of the transport equations is treating C_U and C_T are constant. Then, in a constant property condition, these simplified equations can be integrated as

$$\mu\frac{\mathrm{d}U}{\mathrm{d}y^*} = C_U\frac{y^*}{\Gamma_U} + A_U\frac{1}{\Gamma_U}, \tag{3}$$

$$\mu U = C_U\int\frac{y^*}{\Gamma_U}\,\mathrm{d}y^* + A_U\int\frac{1}{\Gamma_U}\,\mathrm{d}y^* + B_U, \tag{4}$$

$$\frac{\mu}{Pr}\frac{\mathrm{d}\Theta}{\mathrm{d}y^*} = C_T\frac{y^*}{\Gamma_\theta} + A_T\frac{1}{\Gamma_\theta}, \tag{5}$$

$$\frac{\mu}{Pr}\Theta = C_T\int\frac{y^*}{\Gamma_\theta}\,\mathrm{d}y^* + A_T\int\frac{1}{\Gamma_\theta}\,\mathrm{d}y^* + B_T, \tag{6}$$

where A_U, B_U, A_T and B_T are integration constants. Another important assumption is prescribing the variation of the turbulent viscosity μ_t over a wall-adjacent computational-cell as in Fig. 2. For smooth wall heat transfer, μ_t variation is assumed that μ_t is zero for $y^* \leqslant y_v^* = 10.7$ (y_v: the thickness of the viscosity dominated sub-layer) and then increases linearly:

$$\mu_t/\mu = \max\{0, \alpha(y^* - y_v^*)\}, \tag{7}$$

where $\alpha = c_\ell c_\mu = 2.55 \times 0.09$ and μ is the molecular viscosity. Since the theoretical wall-limiting variation of μ_t is proportional to y^3, the AWF does not count a certain amount of turbulent viscosity in the viscous sub-layer. Despite that, its effect is not serious for flow field prediction since the contribution from the molecular viscosity is more significant in the sub-layer. This is also true for the thermal field prediction of fluids whose Pr is less than 1.0. However, in high Pr fluid flows such as oil flows, since the effect of the molecular thermal diffusivity (μ/Pr) becomes very small as illustrated in Fig. 3, it is then necessary to consider the contribution from the turbulent thermal diffusivity inside the sub-layer. (Note that a prescribed constant turbulent Prandtl number Pr_t is assumed in Fig. 3.)

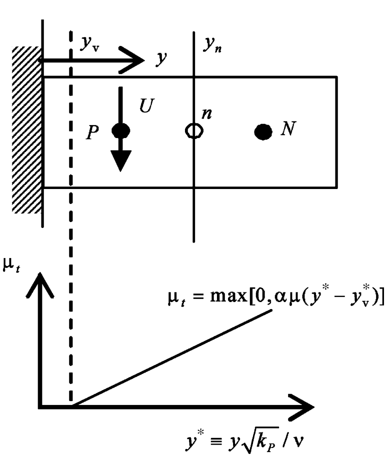

Fig. 2. Near-wall cell arrangement.

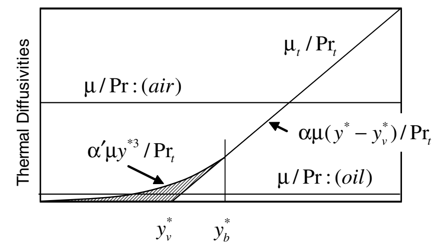

Fig. 3. Near-wall thermal diffusivity distribution.

In order to compensate the thermal diffusivity inside the sub-layer, Gerasimov [13] introduced an *ad hoc* effective molecular Prandtl number as

$$Pr_{\mathrm{eff}} = \frac{Pr}{1 + 0.017Pr(1 + 2.9|F_\varepsilon - 1|)^{1.5}}, \tag{8}$$

where F_ε is a model function. This effective Pr approach was tailored for water flows. Thus, its performance in oil flows whose Pr is over 100 is not guaranteed.

In the present study, such an effective Pr concept is not considered, correcting the profile of μ_t to reproduce the exact wall-limiting behaviour is instead tried. In order to improve the μ_t profile inside the sub-layer, it is assumed that the profile of Eq. (7) is connected to a function: $\alpha' y^{*3}$ at the point y_b^*, as illustrated in Fig. 3.

$$\mu_t/\mu = \begin{cases} \alpha' y^{*3} & \text{for } 0 \leqslant y^* \leqslant y_b^*, \\ \alpha(y^* - y_v^*) & \text{for } y_b^* \leqslant y^*. \end{cases} \tag{9}$$

Thus,

$$\Gamma_\theta = \begin{cases} 1 + \alpha' Pr y^{*3}/Pr_t = \Gamma_{\theta a} & \text{for } 0 \leqslant y^* \leqslant y_b^*, \\ 1 + \alpha Pr(y^* - y_v^*)/Pr_t = \Gamma_{\theta b} & \text{for } y_b^* \leqslant y^*. \end{cases} \tag{10}$$

By referring to the near-wall profile of μ_t in a DNS dataset [14], the value of y_b^* is optimised as $y_b^* = 11.7$ and thus α' is obtainable as

$$\alpha' = \alpha(y_b^* - y_v^*)/y_b^{*3} = \alpha/y_b^{*3}. \tag{11}$$

Using Eq. (10), integration in Eq. (6) can be made. (Although the modification of the model is very simple, its makes the analytical integration a little cumbersome.) As described in Suga et al. [7] the integration constants are obtained by applying boundary conditions at the wall, y_b and the point n. The values at n are determined by interpolation between the calculated node values at P and N, whilst at y_b a monotonic distribution condition is imposed by ensuring that Θ and its gradient should be continuous. Consequently, the wall heat flux q_w can be described as

$$q_w = -\frac{\rho c_p \nu}{Pr}\frac{\mathrm{d}\Theta}{\mathrm{d}y}\bigg|_w = -\frac{\rho c_p \nu}{Pr}\frac{k_P^{1/2}}{\nu}\frac{\mathrm{d}\Theta}{\mathrm{d}y^*}\bigg|_w = -\frac{\rho c_p k_P^{1/2} A_T}{\mu}, \tag{12}$$

where c_p is the specific heat capacity at constant pressure. Using coefficients D_T and E_T, the resultant form of the integration constant A_T can be written as

$$A_T = \{\mu(\Theta_n - \Theta_w)/Pr + C_T E_T\}/D_T, \tag{13}$$

where Θ_w and Θ_n are the wall temperature and the temperature at y_n. In the case of a constant wall heat flux condition, the wall temperature is obtained by rewriting Eqs. (12) and (13) as

$$\Theta_w = \Theta_n + \frac{Prq_w}{\rho c_p k_P^{1/2}} D_T + \frac{PrC_T E_T}{\mu}. \tag{14}$$

When $y_b \leqslant y_n$, with $P_2 = 1/\Gamma_{\theta a}$, $P_2' = 1/\Gamma_{\theta b}$, $y_0 = 0$, $y_1 = y_b$ and $y_2 = y_n$, the coefficients D_T and E_T are

$$D_T = S_2(y_1) - S_2(y_0) + \{S_2'(y_2) - S_2'(y_1)\}\frac{P_2(y_1)}{P_2'(y_1)}, \tag{15}$$

$$E_T = S_1(y_0) - S_1(y_1) + S_1'(y_1) - S_1'(y_2) + \{S_2'(y_1) - S_2'(y_2)\}\frac{P_1(y_1) - P_1'(y_1)}{P_2'(y_1)}, \tag{16}$$

where $P_1 = y^* P_2$, $P_1' = y^* P_2'$, $S_i = \int P_i \, dy^*$ and $S_i' = \int P_i' \, dy^*$.

In the case of $y_n < y_b$, with $y_0 = 0$, $y_1 = y_n$, they are

$$D_T = S_2(y_1) - S_2(y_0), \tag{17}$$

$$E_T = S_1(y_0) - S_1(y_1). \tag{18}$$

(See Appendix A for the results of the integration of $1/\Gamma_{\theta a}$, etc.)

2.2. High Pr AWF for rough wall heat transfer

For rough wall heat transfer, Suga et al. [7] assumed a functional form of Pr_t in the roughness region of $y \leqslant h$ (h: the roughness height) as

$$Pr_t = Pr_t^{\infty} + C_h \max(0, 1 - y^*/h^*), \tag{19}$$

where $Pr_t^{\infty} = 0.9$ is used. Although the following form for C_h was adopted within the roughness elements ($y \leqslant h$):

$$C_h = \frac{5.5}{1 + (h^*/70)^{6.5}} + 0.6, \tag{20}$$

it was only validated in air flows.

Therefore, the coefficient C_h needs re-calibration in high Pr flows and the presently obtained polynomial form is

$$\begin{aligned} &C_h = \max(0, C_3 Pr^3 + C_2 Pr^2 + C_1 Pr + C_0),\\ &C_3 = -0.48/h^* + 0.0013, \quad C_2 = 9.90/h^* - 0.0291,\\ &C_1 = -72.35/h^* + 0.3067, \quad C_0 = 98.98/h^* + 0.2103. \end{aligned} \tag{21}$$

Since the rough wall AWF [7] modifies y_v^* of Eq. (7) as

$$y_v^* = y_{vs}^*\{1 - (h^*/70)^m\} = y_{vs}^* - \delta_v, \tag{22}$$

with $y_{vs}^* = 10.7$ and

$$m = \max\left\{\left(0.5 - 0.4\left(\frac{h^*}{70}\right)^{0.7}\right), \quad \left(1 - 0.79\left(\frac{h^*}{70}\right)^{-0.28}\right)\right\}, \tag{23}$$

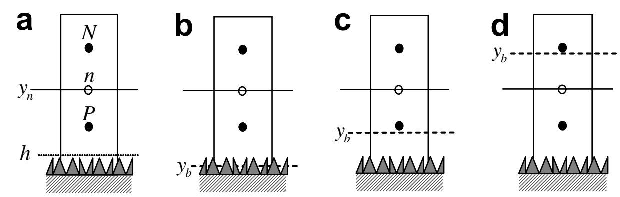

Fig. 4. Near-wall cells over a rough wall: (a) $y_b < 0$, (b) $0 \leqslant y_b \leqslant h$, (c) $h < y_b \leqslant y_n$, (d) $y_n < y_b$.

the turbulent viscosity form of Eq. (9) changes to

$$\mu_t/\mu = \begin{cases} \alpha'(y^* + \delta_v)^3 & \text{for } y^* \leqslant y_b^*,\\ \alpha(y^* - y_v^*) & \text{for } y_b^* < y^*. \end{cases} \tag{24}$$

With the combination of Eqs. (19) and (24), the thermal diffusivity has the following forms:

$$\Gamma_\theta = \begin{cases} 1 + \frac{\alpha' Pr(y^* + \delta_v)^3}{Pr_t^{\infty} + C_h \max(0, 1 - y^*/h^*)} = \Gamma_{\theta c} & \text{for } y^* < y_b^*,\\ 1 + \frac{\alpha Pr(y^* - y_v^*)}{Pr_t^{\infty} + C_h \max(0, 1 - y^*/h^*)} = \Gamma_{\theta d} & \text{for } y_b^* \leqslant y^*. \end{cases} \tag{25}$$

The analytical solutions of energy equations then can be obtained in the four different cases illustrated in Fig. 4 assuming that the wall-adjacent cell height is always greater than the roughness height. The resultant expressions for q_w and A_T are of the same form as those of Eqs. (12)–(14). For cases (a) and (d) of Fig. 4, D_T and E_T have the forms of Eqs. (15) and (16) with some changes. For case (a), they are $P_2 = P_2' = 1/\Gamma_{\theta d}$, $y_0 = 0$, $y_1 = h$ and $y_2 = y_n$. For case (d), they are $P_2 = P_2' = 1/\Gamma_{\theta c}$, $y_0 = 0$, $y_1 = h$ and $y_2 = y_n$.

In cases (b) and (c), D_T and E_T have the following forms:

$$D_T = S_2(y_1) - S_2(y_0) + \{S_2'(y_2) - S_2'(y_1)\}\frac{P_2(y_1)}{P_2'(y_1)} + \{S_2''(y_3) - S_2'(y_2)\}\frac{P_2(y_1)P_2'(y_2)}{P_2'(y_1)P_2''(y_2)}, \tag{26}$$

$$\begin{aligned} E_T = {} & S_1(y_0) - S_1(y_1) + S_1'(y_1) - S_1'(y_2) + \{S_2'(y_1) - S_2'(y_2)\}\frac{P_1(y_1) - P_1'(y_1)}{P_2'(y_1)} + S_1''(y_2) - S_1''(y_3) + \{S_2''(y_2)\\ & - S_2''(y_3)\}\left(\frac{P_1(y_1) - P_1'(y_1)}{P_2'(y_1)} \cdot \frac{P_2'(y_2)}{P_2''(y_2)} + \frac{P_1'(y_2) - P_1''(y_2)}{P_2''(y_2)}\right). \end{aligned} \tag{27}$$

For case (b), $P_2 = 1/\Gamma_{\theta c}$, $P_2' = P_2'' = 1/\Gamma_{\theta d}$, $S_i'' = \int P_i'' \, dy^*$, $y_0 = 0$, $y_1 = y_b$, $y_2 = h$, and $y_3 = y_n$. For case (c), $P_2 = P_2' = 1/\Gamma_{\theta c}$, $P_2'' = 1/\Gamma_{\theta d}$, $y_0 = 0$, $y_1 = h$, $y_2 = y_b$, and $y_3 = y_n$. (See Appendix A for the results of the integration of $1/\Gamma_{\theta c}$, etc.)

3. Application results

3.1. Smooth wall heat transfer

In order to confirm the effects of the corrected turbulent viscosity on the flow fields, Fig. 5 compares the mean velocity profiles in turbulent channel flows at the bulk Reynolds number, $Re = 10^5$. (The standard high Reynolds number

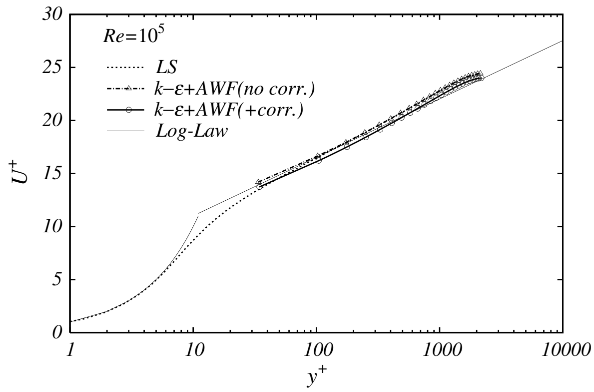

Fig. 5. Mean velocity profiles in turbulent smooth channel flows.

$k-\varepsilon$ model [5] and the eddy diffusivity model with $Pr_t = 0.9$ are used for the computation of the core fields of the present study.) Although the result by the μ_t correction almost perfectly lies on the log-law line and there can be seen a slight discrepancy between the results with and without the correction, both the results well accord with the LRN Launder-Sharma (LS) $k-\varepsilon$ model [10] and the log-law profiles. (The meshes used for the AWF and the LRN computations have respectively 50 and 100 node points in the wall normal direction. Their first cell heights are $y^+ \simeq 30$ and $y^+ \simeq 0.2$, respectively.) This confirms that the correction in the momentum equation may not be totally necessary for engineering flow field computations and thus the present study does not employ the correction for the flow field AWF. This means that the correction of μ_t is made only in the energy equation in the present study.

Fig. 6 clearly indicates that without the correction, the AWF does not properly reproduce the logarithmic temperature profiles in high Pr flows ($Pr \geqslant 5.0$). Note that the experimentally suggested logarithmic distribution by Kader [15] for a wide range of Pr is

$$\Theta^+ = 2.12\ln(y^+Pr) + (3.85Pr^{1/3} - 1.3)^2. \tag{28}$$

In the case of $Pr = 0.71$, the profiles of the AWF with and without the correction are virtually identical and confirm that the near-wall correction of μ_t is effective for flows at $Pr > 1.0$.

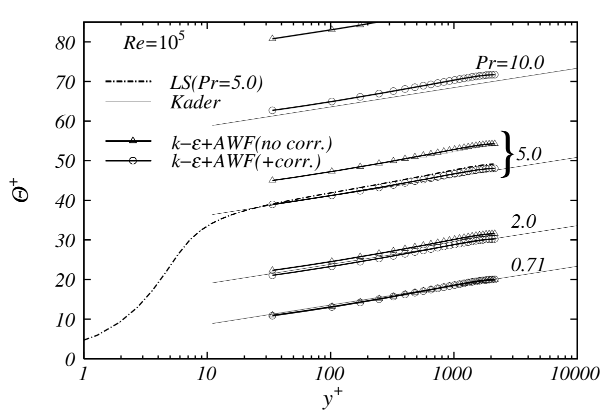

Fig. 6. Mean temperature profiles in turbulent smooth channel flows.

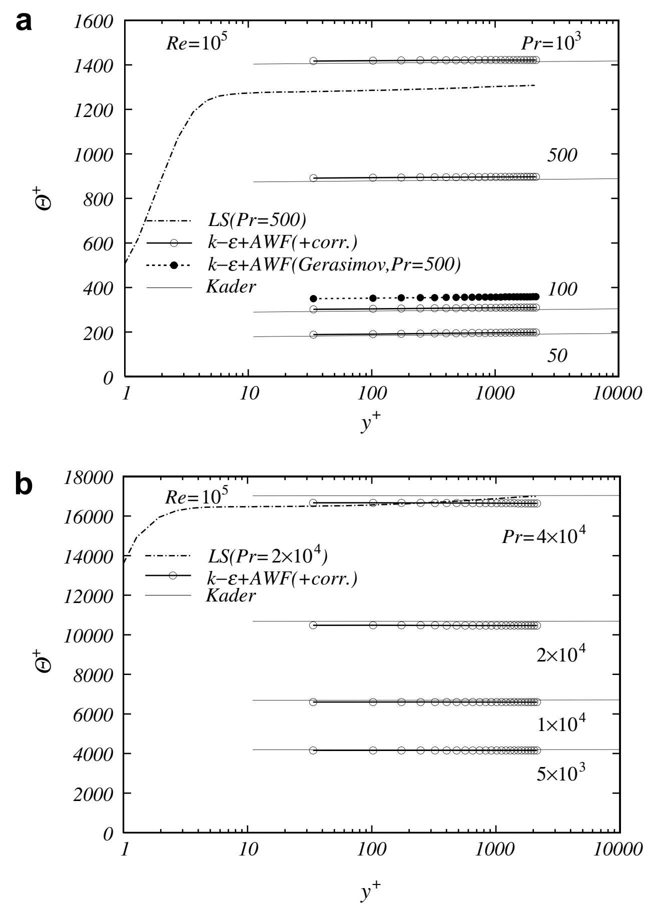

Fig. 7. Mean temperature profiles in turbulent smooth channel flows at higher Pr.

As shown in Fig. 7a, the corrected AWF proves its good performance in the range of $50 \leqslant Pr \leqslant 10^3$. However, both the LRN LS model and the AWF with Gerasimov's [13] effective molecular Prandtl number scheme fail to predict the thermal field at $Pr = 500$. The former predicts the temperature too high and the latter does too low. Fig. 7b also confirms that the corrected AWF performs well up to $Pr = 4 \times 10^4$ though the LRN LS model predicts the thermal field too high. Note that the same grid resolution as that for $Pr = 5.0$ is used in the LRN computations. This reasonably implies that the grid resolution used is too coarse and a much finer grid is needed for such a high Pr computations by the LRN models. Obviously, it highlights the merit of using the AWF which does not require a finer grid resolution for a higher Pr flow.

3.2. Rough wall heat transfer

Fig. 8 compares the predicted temperature fields of turbulent rough channel flows of $h/D = 0.005$, 0.01 and 0.03, (D: channel height). In the cases of $h/D = 0.005$, 0.01, the corresponding roughness Reynolds numbers are respectively $h^+ \simeq 30,60$ which are in the transitional roughness regime, while $h/D = 0.03$ corresponds to $h^+ \simeq 220$ which

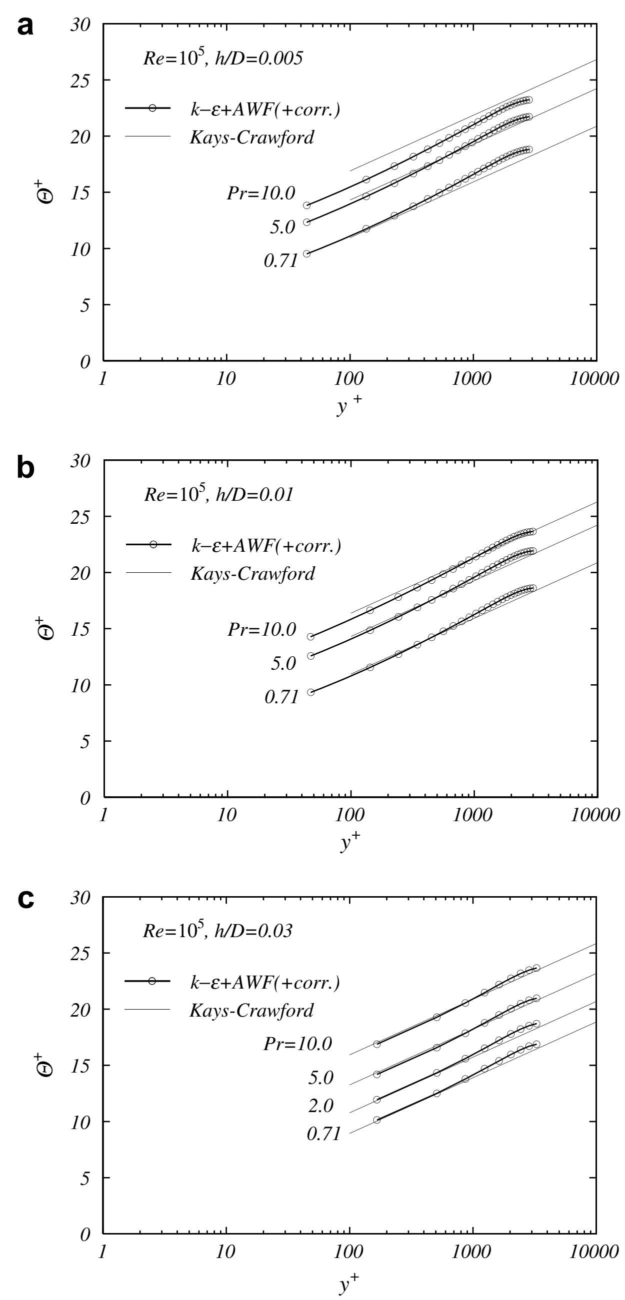

Fig. 8. Mean temperature profiles in turbulent rough channel flows.

is well in the fully rough regime. For each roughness case, it is obvious that the corrected AWF reasonably well reproduces the temperature distribution for rough walls [16]:

$$\Theta^+ = \frac{1}{0.8h^{+^{-0.2}}Pr^{-0.44}} + \frac{Pr_t}{\kappa}\ln\frac{32.6y^+}{h^+}, \tag{29}$$

where $Pr_t = 0.9$ and $\kappa = 0.418$. This correlation is based on the experiments [17] of $Pr = 1.20$–5.94 at the order of Re is 10^4–10^5. Since experimental data for high Pr rough wall turbulent heat transfer are limited in the literature (as far as the author knows), discussions of flows at $Pr > 10$ have not been made.

4. Conclusions

The analytical wall-function for thermal fields, which had been developed for application to problems with smooth and rough wall air flows, has been extended to account for the effects of the high fluid Prandtl number on turbulent heat transfer. The concluding remarks of the present study are:

(1) By linking to the correct near-wall variation of turbulent viscosity: $\mu_t \propto y^3$, the improved scheme has proven its good performance in fully developed turbulent channel flows over a wide range of Prandtl numbers up to $Pr = 4 \times 10^4$, for smooth wall cases.
(2) For flow fields and thermal fields at $Pr \leqslant 1$, it is not totally necessary to employ the correct near-wall variation of turbulent viscosity.
(3) For rough wall cases, it is confirmed that the amended model function of Pr_t inside roughness elements enables the AWF to perform well in high Pr flows at least at $Pr \leqslant 10$.

Since the base model was validated in a wide range of complex air flow fields, the present model is reasonably thought to be useful in complex geometries as well. Further tests in such fields with high Pr fluids, however, should be made in the future.

Acknowledgements

The author thanks Professors B.E. Launder, H. Iacovides and Dr. T.J. Craft of the University of Manchester for their fruitful discussions and comments on the development of the AWF. This work was financially supported by the Japan Society for the Promotion of Science through a Grant-in-Aid for Scientific Research (B) (No. 18360050).

Appendix A

The integrals of the functions are

$$\int \frac{1}{\Gamma_{\theta a}}\,dy^* = \int \frac{1}{1+\frac{\alpha' Pr y^{*3}}{Pr_t}}\,dy^* = \frac{a}{3}\left\{\frac{1}{2}\ln\frac{(y^*+a)^2}{y^{*2}-ay^*+a^2} + \sqrt{3}\tan^{-1}\frac{2y^*-a}{a\sqrt{3}}\right\}, \tag{30}$$

$$\int \frac{y^*}{\Gamma_{\theta a}}\,dy^* = \int \frac{y^*}{1+\frac{\alpha' Pr y^{*3}}{Pr_t}}\,dy^* = \frac{a^2}{3}\left\{-\frac{1}{2}\ln\frac{(y^*+a)^2}{y^{*2}-ay^*+a^2} + \sqrt{3}\tan^{-1}\frac{2y^*-a}{a\sqrt{3}}\right\}, \tag{31}$$

$$\int \frac{1}{\Gamma_{\theta b}}\,dy^* = \int \frac{1}{1+\frac{\alpha Pr (y^*-y_v^*)}{Pr_t}}\,dy^* = \frac{1}{\alpha_\theta}\ln|1+\alpha_\theta(y^*-y_v^*)|, \tag{32}$$

$$\int \frac{y^*}{\Gamma_{\theta b}} \mathrm{d}y^* = \int \frac{y^*}{1+\frac{\alpha \mathrm{Pr}(y^*-y_v^*)}{Pr_\mathrm{t}}} \mathrm{d}y^* = \frac{y^*}{\alpha_\theta} - \frac{1-\alpha_\theta y_v^*}{\alpha_\theta^2} \ln|1+\alpha_\theta(y^*-y_v^*)|, \tag{33}$$

$$\int \frac{1}{\Gamma_{\theta d}} \mathrm{d}y^* = \int \frac{1}{1+\frac{\alpha Pr(y^*-y_v^*)}{\mathrm{Pr}_\mathrm{t}^\infty + C_h \max(0,1-y^*/h^*)}} \mathrm{d}y^* = -\frac{\beta_T y^*}{\alpha_T-\beta_T} + \left\{\frac{\beta_T \lambda_\mathrm{b}}{(\alpha_T-\beta_T)^2} + \frac{1+\beta_T h^*}{\alpha_T-\beta_T}\right\} \times \ln|(\alpha_T-\beta_T)y^* + \lambda_\mathrm{b}|, \tag{34}$$

$$\int \frac{y^*}{\Gamma_{\theta d}} \mathrm{d}y^* = \int \frac{y^*}{1+\frac{\alpha Pr(y^*-y_v^*)}{Pr_\mathrm{t}^\infty + C_h \max(0,1-y^*/h^*)}} \mathrm{d}y^* = -\frac{\beta_T y^{*2}}{2(\alpha_T-\beta_T)} + \left\{\frac{\beta_T \lambda_\mathrm{b}}{(\alpha_T-\beta_T)^2} + \frac{1+\beta_T h^*}{\alpha_T-\beta_T}\right\} y^* - \left\{\frac{\beta_T \lambda_\mathrm{b}^2}{(\alpha_T-\beta_T)^3} + \frac{\lambda_\mathrm{b}(1+\beta_T h^*)}{(\alpha_T-\beta_T)^2}\right\} \times \ln|(\alpha_T-\beta_T)y^* + \lambda_\mathrm{b}|, \tag{35}$$

where $\alpha_\theta = \alpha Pr/Pr_\mathrm{t}$, $\alpha_T = \alpha Pr/Pr_\mathrm{t}^\infty$, $a = (\alpha' Pr/Pr_\mathrm{t})^{-1/3}$,

$$\beta_T = \begin{cases} C_h/(Pr_\mathrm{t}^\infty h^*) & \text{for } y \leqslant h, \\ 0 & \text{for } h < y, \end{cases}$$

$\lambda_\mathrm{b} = 1 - \beta_T h^* - \alpha y_v^*$. (Note that integration constants are neglected in the results.)

$$\int \frac{1}{\Gamma_{\theta c}} \mathrm{d}y^* = \int \frac{1}{1+\frac{\alpha' Pr(y^*+\delta_v)^3}{\mathrm{Pr}_\mathrm{t}^\infty + C_h \max(0,1-y^*/h^*)}} \mathrm{d}y^* = \frac{\zeta}{\alpha'_T}\Big[-\Big\{\eta_c \beta_T - (\eta_a - \eta_\mathrm{b})(1+\beta_T h^*) - \frac{\eta_\mathrm{b}}{2}(1+\beta_T[h^*+\eta_a])\Big\}\Phi(y) - \frac{1+\beta_T(h^*+\eta_a)}{2} \ln|y^{*2} + \eta_\mathrm{b} y^* + \eta_c| + \{1+\beta_T(h^*+\eta_a)\}\ln|y^*+\eta_a|\Big], \tag{36}$$

$$\int \frac{y^*}{\Gamma_{\theta c}} \mathrm{d}y^* = \int \frac{y^*}{1+\frac{\alpha' Pr(y^*+\delta_v)^3}{Pr_\mathrm{t}^\infty + C_h \max(0,1-y^*/h^*)}} \mathrm{d}y^* = \frac{\zeta}{\alpha'_T}\Big[\Big\{\eta_c(1+\beta_T[h^*+\eta_a]) - \frac{\eta_\mathrm{b}}{2}(\beta_T[\eta_a\eta_\mathrm{b} - \eta_c] + \eta_a[1+\beta_T h^*])\Big\}\Phi(y) + \frac{1}{2}\{\beta_T[\eta_a\eta_\mathrm{b} - \eta_c] + \eta_a(1+\beta_T h^*)\} \ln|y^{*2} + \eta_\mathrm{b} y^* + \eta_c| - \eta_a\{1+\beta_T(h^*+\eta_a)\}\ln|y^*+\eta_a|\Big], \tag{37}$$

where $\alpha'_T = \alpha' Pr/Pr_\mathrm{t}^\infty$, $p = -\beta_T/(3\alpha'_T)$, $q = \{1+\beta_T(h^*+\delta_v)\}/(2\alpha'_T)$,

$$\xi = \begin{cases} \left(-q+\sqrt{q^2+p^3}\right)^{1/3} + \left(-q-\sqrt{q^2+p^3}\right)^{1/3} \\ \quad \text{if } q^2+p^3 \geqslant 0, \\ 2\sqrt{-p}\cos\left[\frac{1}{3}\cos^{-1}\left(\frac{q}{p\sqrt{-p}}\right)\right] \\ \quad \text{if } q^2+p^3 < 0, \end{cases} \tag{38}$$

$\eta_a = \delta_v - \xi$, $\eta_\mathrm{b} = 2\delta_v + \xi$, $\eta_c = \delta_v^2 + \delta_v\xi + \xi^2 + 3p$, $\zeta = 1/\{\eta_a(\eta_a - \eta_\mathrm{b}) + \eta_c\}$, and

$$\Phi(y) = \begin{cases} -\frac{2}{\eta_\mathrm{b}+2y^*} \\ \quad \text{if } \eta_\mathrm{b}^2 - 4\eta_c = 0, \\ \frac{2}{\sqrt{-\eta_\mathrm{b}^2+4\eta_c}} \tan^{-1}\left(\frac{\eta_\mathrm{b}+2y^*}{\sqrt{-\eta_\mathrm{b}^2+4\eta_c}}\right) \\ \quad \text{if } \eta_\mathrm{b}^2 - 4\eta_c < 0, \\ \frac{2}{\sqrt{\eta_\mathrm{b}^2-4\eta_c}} \ln\left|\frac{\eta_\mathrm{b}+2y^*-\sqrt{\eta_\mathrm{b}^2-4\eta_c}}{\eta_\mathrm{b}+2y^*+\sqrt{\eta_\mathrm{b}^2-4\eta_c}}\right| \\ \quad \text{if } \eta_\mathrm{b}^2 - 4\eta_c > 0. \end{cases} \tag{39}$$

References

[1] M.M. Rogers, N.N. Mansour, W.C. Reynolds, An algebraic model for the turbulent flux of a passive scalar, J. Fluid Mech. 203 (1989) 77–101.

[2] K. Suga, K. Abe, Nonlinear eddy viscosity modelling for turbulence and heat transfer near wall and shear-free boundaries, Int. J. Heat Fluid Flow 21 (1) (2000) 37–48.

[3] J. Herrero, F.X. Grau, J. Grifoll, F. Giralt, A near wall $k-\varepsilon$ formulation for high Prandtl number heat transfer, Int. J. Heat Mass Transfer 34 (3) (1991) 711–721.

[4] R.M.C. So, T.P. Sommer, A near-wall eddy conductivity model for fluids with different Prandtl numbers, ASME J. Heat Transfer 116 (1994) 844–854.

[5] B.E. Launder, D.B. Spalding, The numerical computation of turbulent flows, Comp. Meth. Appl. Mech. Engng. 3 (1974) 269–289.

[6] T.J. Craft, A.V. Gerasimov, H. Iacovides, B.E. Launder, Progress in the generalization of wall-function treatments, Int. J. Heat Fluid Flow 23 (2002) 148–160.

[7] K. Suga, T.J. Craft, H. Iacovides, An analytical wall-function for turbulent flows and heat transfer over rough walls, Int. J. Heat Fluid Flow 27 (2006) 852–866.

[8] D. Apsley, CFD calculation of turbulent flow with arbitrary wall roughness, Flow Turbulence Combust. 78 (2007) 153–175.

[9] M. Popovac, K. Hanjalic, Compound wall treatment for RANS computation of complex turbulent flows and heat transfer, Flow Turbulence Combust. 78 (2007) 177–202.

[10] B.E. Launder, B.I. Sharma, Application of the energy-dissipation model of turbulence to the calculation of flow near a spinning disc, Lett. Heat Mass Transfer 1 (1974) 131–138.

[11] T.J. Craft, B.E. Launder, K. Suga, Development and application of a cubic eddy-viscosity model of turbulence, Int. J. Heat Fluid Flow 17 (1996) 108–115.

[12] N. Kasagi, N. Shikazono, Contribution of direct numerical simulation to understanding and modelling turbulent transport, Proc. R. Soc. Lond. A 451 (1995) 257–292.

[13] A.V. Gerasimov, Development and validation of an analytical wall-function strategy for modelling forced, mixed and natural convection phenomena, Ph.D. Thesis, UMIST, Manchester, UK 2003.

[14] K. Iwamoto, Database of fully developed channel flow, THTLAB Internal Report, No. ILR-0201, Dept. Mech. Eng., The University of Tokyo, Tokyo, Japan 2002.
[15] B.A. Kader, Temperature and concentration profiles in fully turbulent boundary layers, Int. J. Heat Mass Transfer 24 (1981) 1541–1544.
[16] W.M. Kays, M.E. Crawford, Convective Heat and Mass Transfer, third ed., McGraw-Hill, 1993, pp. 298–301.
[17] D.F. Dipprey, R.H. Sabersky, Heat and momentum transfer in smooth and rough tubes at various Prandtl numbers, Int. J. Heat Mass Transfer 6 (1963) 329–353.